Advances in Science and Technology Research Journal

Advances in Science and Technology Research Journal 2024, 18(3), 45–57
https://doi.org/10.12913/22998624/185618
ISSN 2299-8624, License CC-BY 4.0

Received: 2024.02.21
Accepted: 2024.03.04
Published: 2024.04.20

The Use of Artificial Intelligence for Quality Assessment of Refill Friction Stir Spot Welded Thin Joints

Andrzej Kubit[1], Grzegorz Kłosowski[2*], Wojciech Berezowski[3]

[1] Department of Manufacturing and Production Engineering, Rzeszow University of Technology, ul. Powstańców Warszawy 8, 35-959 Rzeszów, Poland

[2] Faculty of Management, Lublin University of Technology, ul. Nadbystrzycka 38 D, 20-618 Lublin, Poland

[3] Department of Mechanics and Machine Building, State Academy of Applied Sciences in Krosno, ul. Żwirki i Wigury 9A, 38-400 Krosno, Poland

* Corresponding author's e-mail: g.klosowski@pollub.pl

ABSTRACT

This paper presents a machine learning and image segmentation based advanced quality assessment technique for thin refill friction stir spot welded (RFSSW) joints. In particular, the research focuses on developing a predictive support vector machines (SVM) model. The purpose of this model is to facilitate the selection of RFSSW process parameters in order to increase the shear load capacity of joints. In addition, an improved weld quality assessment algorithm based on optical analysis was developed. The research methodology includes specimen preparation stages, mechanical tests, and algorithmic analysis, culminating in a machine learning model trained on experimental data. The results demonstrate the effectiveness of the model in selecting welding process parameters and assessing weld quality, offering significant improvements compared to standard techniques. The optimized SVM model, employing the radial basis function (RBF) kernel, achieved a lower root mean square error of 257.9 and a high correlation coefficient of 0.95, indicating a strong linear relationship between the predicted and actual shear load capacities. This research not only proposes a novel approach to optimizing welding parameters but also facilitates automatic quality assessment, potentially revolutionizing and spreading the application of the RFSSW technique in various industries.

Keywords: friction welding, prediction, SVM, image classification.

INTRODUCTION

Refill friction stir spot welding (RFSSW) is a relatively new solid-state butt-welding technique that uses friction and the joining of materials induced by a rotating welding tool [1]. Friction between the welded elements creates heat, which causes their plastic fusion. RFSSW is similar to another technique called friction stir welding (FSW), which is used for linear welding [2, 3]. Currently, the most used welding technique is resistance spot welding (RSW) [4]. RFSSW differs from traditional thermal welding techniques in that it does not require melting the metal. This prevents cracks, pores, oxidation, and other defects associated with the thermal welding cycle [5]. The RFSSW method is more tolerant when combining metal plates with different surfaces. The riveting method is a conventional technique used for joining materials and is prevalent in various industries such as machine building, steel structures, aerospace, and automotive sectors [6]. This technique's primary benefit is its advantageous cost-quality ratio [7]. Despite its versatility and proven effectiveness, riveting has a number of disadvantages and potential problems, especially when compared to more modern joining methods such as friction welding [8]. Riveting has drawbacks such as high time and labor requirements, lower join tightness compared to welding, the necessity to reach both sides of the structural system being joined, and a higher

likelihood of corrosion and damage. Rivets create concentrated loads in the structure, which can cause stress concentration and raise the likelihood of fatigue cracking, particularly in environments with high dynamic loads [9]. The technique imposes significant limitations on structural design due to the requirements for rivet placement and access to rivet sites. Replacing riveting with the RFSSW technique can eliminate many of these problems [10]. Various factors limit the widespread adoption of RFSSW in the industry. These include challenges related to choosing the best RFSSW process parameters and accurately evaluating the weld quality [11, 12]. The efficiency of manufacturing processes is closely linked to the degree of automation they possess [13,14]. Information technologies, particularly those utilizing machine learning, are becoming increasingly significant in the field of manufacturing control. Dynamic development focuses on methods like artificial neural networks, elastic net, support vector machine, LSTM, and other related techniques [15, 16]. This study aims to develop a new predictive model based on machine learning to optimize the selection of RFSSW process parameters for achieving maximum shear load capacity in the joint [17, 18]. Moreover, the research developed an improved algorithm enabling a percentage assessment of the quality of the RFSSW joint based on optical analysis of the weld. The research is aimed at increasing the effectiveness of the RFSSW method, especially in relation to riveting and resistance welding, which will contribute to increasing the scale of applications of the RFSSW technique in industry. The paper is structured into several sections, beginning with an introduction that sets the context and objectives of the research. It proceeds with a literature review, discussing previous studies relevant to RFSSW and artificial intelligence applications in welding. The methodology section details the experimental setup, materials used, and procedure for data collection and analysis. Results are presented with a comprehensive discussion, interpreting the findings in the context of the research goals. The article concludes with a summary of the outcomes, implications for the industry, and suggestions for future research. This structure ensures a logical flow from background to findings, facilitating reader comprehension.

MATERIALS AND METHODS

This section details the procedure for testing a lap joint created through the RFSSW technique. It includes details about the materials, devices, and tools utilized for sample preparation, along with the procedure for testing the shear load capacity of the joint. This section outlines algorithmic methods for predicting optimal process parameters and evaluating joint quality optically.

Technical description of RFSSW samples

The joint consisted of two sheets of different thickness, corresponding to the stringer and skin in a thin-walled aerospace structure. It was assumed that both elements would be made of the same duralumin alloy, EN AW-7075-T6 Alclad, commonly used in aircraft structures. Alloy EN AW-7075-T6 Alclad is characterized by high static and fatigue strength, as well as low weight. Its ultimate tensile stress (R_m) is 540 MPa, and the yield stress ($R_{p0.2}$) ranges from 460 to 475 MPa. The main alloying additions are zinc (5.6%), magnesium (2.61%), and copper (1.35%). Despite many advantages, this material is difficult to form and weld and has relatively low corrosion resistance. For this reason, sheets used in the construction of thin-walled aircraft structures are clad with a thin layer of technical aluminum (approximately 5% of the thickness). Plating protects the alloy against intergranular corrosion by creating a layer of aluminum oxide on the surface. The research focused on the lap joint of sheets of varying thickness, imitating the joint of the stringer and the covering in a thin-walled aircraft structure. EN AW-7075-T6 Alclad sheets were used with thicknesses corresponding to real aviation applications.

Figure 1 shows the refill friction stir spot welding process flow. The process can be divided into four main stages: landing, plunging, refilling, and retreating. In the first stage, the compression ring is placed on the top surface of the sheet, and the sleeve and pin begin to rotate and rub against the sheet, which plasticizes the metal and facilitates penetration. To push the plasticized metal into the cylindrical space that the pin's upward movement creates, the sleeve and pin reciprocate. Once a certain plunge depth is reached, the directions of movement of the sleeve and pin begin to reverse, which causes the plastic metal to be squeezed back through the sleeve. Finally, the welding head is removed from the joined work pieces. The sleeve, which plunges into the base metal plate, plays a crucial role in the conventional RFSSW process. In the described experiments, a refill friction stir

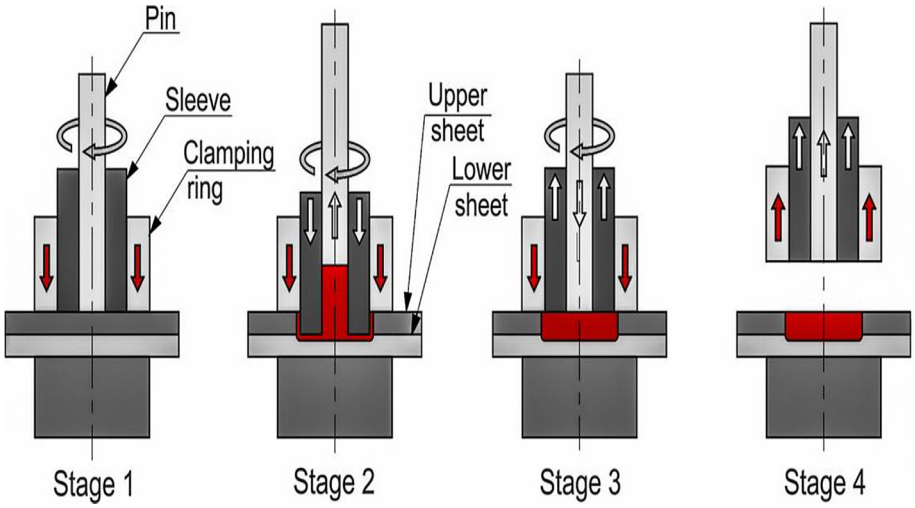

Figure 1. Phases of the refill friction stir spot welding process

spot welding machine type RPS100 from Harms & Wende GmbH & Co. KG was used. The device is characterized by a spindle speed of 3,000 rpm, an output power of 2.2 kW, plunge speeds up to 3.6 mm/s, and a maximum force of 11,000 N. Figure 2 shows the welding tool. Its purpose is to join two sheets of aluminum in an overlapping configuration, with the top sheet having greater thickness. This arrangement of sheets contributes to better joint load capacity. Samples consisting of two plates (sheets) were welded. The dimensions of the top plate (length × width × thickness) are 120 × 30 × 1.6 mm. The dimensions of the bottom plate are 120 × 30 × 0.8 mm. The welding tool was used on the thicker (i.e., upper) side of the plate.

Shear load capacity test of RFSSW joint

Figure 3 shows a diagram of the installation for testing the load capacity of the RFSSW joint. The test included shear tests performed using a Zwick Roell Z-100 universal testing machine with a transverse travel speed of 5 mm/min at room temperature, in accordance with the DIN EN ISO 14273 standard. In these tests, depending on the plunge depth of the tool, there are three types of joint damage: plug crack, shear crack, and plug-shear crack. The aim of the research was to select the parameters of the RFSSW welding process in order to maximize the load capacity of the joint. The selected input parameters were: tool rotational speed (rpm), tool plunge

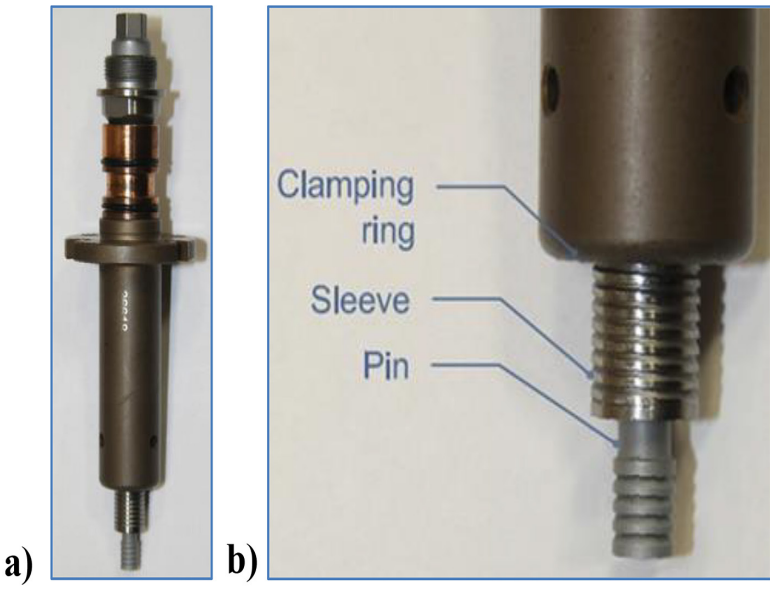

Figure 2. The welding tool: (a) general view, (b) close-up

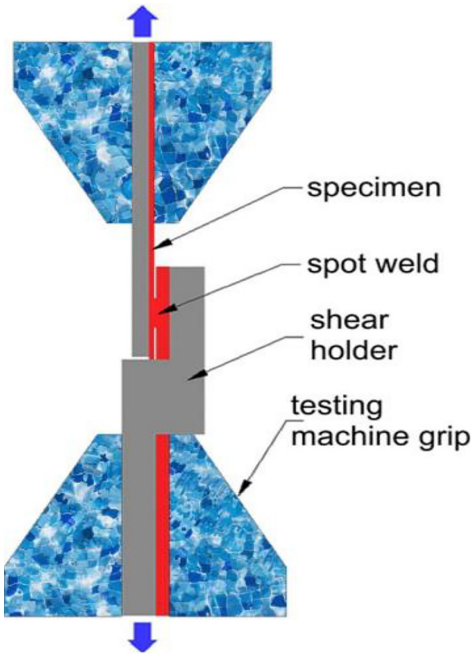

Figure 3. Diagram for the shear test

depth (mm), and welding time (s). The selection of these three parameters results from the fact that previous research indicates a significant impact of both the tool rotational speed, welding time, and plunge depth on the mechanical strength and quality of the microstructure of the joint.

Research methodology

To achieve the research goal, 50 samples of joints made using the RFSSW method using identical metal plates were prepared. Each RFSSW sample was fabricated with different welding process parameters (tool rotational speed, tool plunge depth, and welding time). The samples were then photographed both from above and in cross-section. It should be noted that a cross-section photograph requires the destruction of the welded structure. Therefore, in real conditions, optical quality assessment is carried out only on the basis of a photo of the weld in a top view. The evaluation of cross-sectional photographs was performed only for the purpose of validating the optical method. In the next phase of the research, a machine learning model was trained based on the support vector machine (SVM) method, enabling the optimal selection of welding parameters using the RFSSW method. In the next stage, an algorithmic method for quality control of the made joint was developed, using photos of welds.

Optimization of the RFSSW process using the SVM method

The support vector machines method was used to optimize the parameters of the friction welding process. SVMs are a strong machine learning algorithm that is able to be implemented to classify as well as regress [19]. For SVMs, it does this by finding the hyperplane that separates the classes of data. This margin is defined as the distance between the hyperplane and the hyperpoints, or support vectors, of the data points nearest to it for each class.

The SVMs have some strengths that make them good for small datasets. The first is the fact that the SVM is more immune from overfitting in comparison to many other machine learning algorithms, like, for example, neural networks. This is because SVM only gives attention to the support vectors, and the support vectors are the most critical points in the data that actually categorize the decision boundary. Second, SVM is more efficient compared to other machine learning algorithms. This is because SVMs only require a few support vectors to define the decision boundary. This makes SVM suitable for real-time applications. Thirdly, it is more interpretable than other machine learning algorithms. The interpretability of SVMs might be linked to the type of model. Since SVMs represent a simple linear model, it will not be hard to understand why a certain class is predicted by the SVM, which is helpful to debug and improve the model. In general, SVMs are a good choice for a problem of machine learning in which the dataset is small. They are more resistant to overfitting, more efficient, and more interpretable compared with other machine learning algorithms. MATLAB R2023b software was used to train the SVM model. Below is a detailed description of how the SVM model works.

Input data

The SVM model is represented by a function that takes predictor data x and response data x as vectors or matrices. In this case, the variable x is a 50 × 3 matrix in which the columns are: tool rotational speed, tool plunge depth and welding time, respectively. The 50 rows of the x matrix contain the observations. Table 1 presents a set of 50 measurements determining the parameters of the RFSSW process for 50 specimens.

Kernel function

SVM uses a kernel function *K* to map the input data into a higher-dimensional space where the data is linearly separable. The three popular kernel functions were tested: linear, polynomial, and radial basis function (RBF) [20]. The linear kernel function can be described by formula

$$K(x, y) = x^T y \quad (1)$$

where: *x* and *y* are data vectors.

Finally, the linear type of kernel was used in the model. In the research also other kernel models were tested, namely polynomial and RBF. The polynomial kernel is described by the formula

$$K(x, y) = (x^T y + c)^d \quad (2)$$

where: *c* is a constant, *d* is the degree of the polynomial.

The function (3) refers to RBF method

$$K(x, y) = \exp\left(-\gamma \left|\left|x - y\right|\right|^2\right) \quad (3)$$

where: *y* is a scaling parameter.

Optimization

SVM solves an optimization problem that involves minimizing a cost function *L*

$$L = \frac{1}{2}\left|\left|w\right|\right|^2 + C\sum_{i=1}^{n}(\xi_i + \xi_i^*) \quad (4)$$

where: *w* is the weight vector, ξ and ξ^* are slack variables, *C* is a regularization parameter, and *n* is the number of samples.

Model

After optimization, the SVM model is represented by formula (5)

$$f(x) = \mathrm{w}^{\mathrm{T}}\phi(x) + b \quad (5)$$

where: w^T is the weight vector, $\phi(x)$ is the feature mapping function, and *b* is the bias term.

Prediction

For a new data point x', the SVM model prediction is given by (6)

$$y' = f(x') = \sum_{i=1}^{n} \alpha_i K(x_i, x') + b \quad (6)$$

where: α are the Lagrange multipliers, and is the kernel function.

Tuning model parameters

The support vector machine model for regression is also known as Support Vector Regression. It employs a mathematical framework that incorporates several key parameters, including BoxConstraint, KernelScale, and Epsilon (ϵ). The objective of SVM is to construct a function that accurately predicts the real value for an input , while minimizing prediction error and allowing deviations smaller than ϵ In the Equation 5, $\phi(x)$ denotes a function that maps input *x* into a higher-dimensional space affected by KernelScale. The key parameters of the objective SVM function are Epsilon, BoxConstraint and KernelScale.

Epsilon ϵ is used in the epsilon-insensitive loss function

$$Loss\big(y, f(x)\big) = max(0, |y - f(x)| - \epsilon) \quad (7)$$

where: *y* is the true value, *f(x)* is the predicted value, ϵ is a predetermined error tolerance threshold.

If the difference between the true value and the predicted value is less than ϵ, the loss is zero. Otherwise, the loss is equal to the difference between the absolute error and ϵ. Epsilon specifies the width of the "no-penalty" band around the regression function, within which errors are not penalized. This parameter directly affects the model's flexibility in fitting the training data.

BoxConstraint (*C*) in formula (4) is a regularization parameter that controls the trade-off between maintaining the ϵ-margin and maximizing the margin between different data points. A higher *C* value pushes the model to fit the training data more precisely, which can lead to overfitting. It determines the "hardness" of the error margin in the SVR model.

The KernelScale (*y* for RBF) influences the kernel function, enabling the model to handle non-linearities. For the RBF kernel, *y* controls the "width" of the Gaussian function's bell, impacting the model's complexity and its ability to capture dependencies in the data.

SVM often utilizes kernel functions to project input data into a higher-dimensional space, making it easier to find a linear separator (for regression, a line of best fit). An example is the RBF, defined as Equation (3), where is the inverse of KernelScale.

Figure 4 illustrates the process of optimizing the parameters of the SVM function. The process involved 30 iterations. Formula (8) represents the optimized fitness function, which aims to minimize the objective.

$$\text{Min objective} = \log(1 + Loss) \quad (8)$$

Table 1. RFSSW process parameters and joint shear load capacity

Specimen #	Inputs			Output
	Tool rotational speed (rpm)	Plunge depth (mm)	Welding time (s)	Shear load capacity (N)
1	2800	1.5	1.5	7805
2	2800	1.5	2.5	7805
3	2800	1.5	3.5	7035
4	2800	1.7	1.5	7060
5	2800	1.7	2.5	6980
6	2800	1.7	3.5	6920
7	2800	1.9	1.5	6210
8	2800	1.9	2.5	5280
9	2800	1.9	3.5	5080
10	2400	1.5	1.5	7170
11	2400	1.5	2.5	6470
12	2400	1.5	3.5	7640
13	2400	1.7	1.5	6540
14	2400	1.7	2.5	6020
15	2400	1.7	3.5	7110
16	2400	1.9	1.5	5400
17	2400	1.9	2.5	5700
18	2400	1.9	3.5	7080
19	2000	1.5	1.5	6850
20	2000	1.5	2.5	6980
21	2000	1.5	3.5	7010
22	2000	1.7	1.5	6740
23	2000	1.7	2.5	6640
24	2000	1.7	3.5	6980
25	2000	1.9	1.5	5670
26	2000	1.9	2.5	5450
27	2000	1.9	3.5	7390
28	2200	1.6	2	6703
29	2200	1.7	2	8196
30	2200	1.5	2.5	6457
31	2200	1.7	3	6705
32	2400	1.6	2	6367
33	2400	1.7	2	6573
34	2400	1.6	2.5	6830
35	2400	1.8	2.5	5830
36	2400	1.5	3	6556
37	2400	1.6	3	6584
38	2400	1.7	3	6451
39	2400	1.8	3	5215
40	2600	1.6	2	7315
41	2600	1.7	2	6671
42	2600	1.8	2	6156
43	2600	1.5	2.5	6892
44	2600	1.6	2.5	7232
45	2600	1.7	2.5	6748
46	2600	1.8	2.5	6166
47	2600	1.5	3	6141
48	2600	1.6	3	7682
49	2600	1.7	3	6341
50	2600	1.8	3	6916

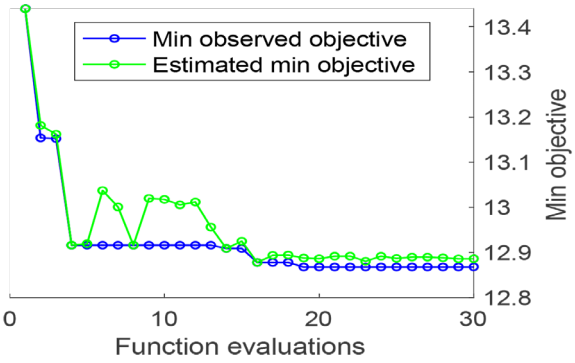

Figure 4. Min objective vs. Number of function evaluations

As it was said, in the context of SVM, Box-Constraint, KernelScale, and Epsilon are critical hyperparameters adjusted to optimize the model's performance. Their optimal values are typically determined using methods like grid search or Bayesian optimization, aiming to minimize prediction error on validation or test sets while preventing overfitting. This nuanced balance between accuracy and generalizability is pivotal for crafting robust regression models capable of tackling real-world data challenges.

Training the SVM model

A set of 50 measurements that determine the parameters of the RFSSW process for 50 specimens is listed in Table 1. The independent (input) variables are: spindle revolutions (rpm), plunge depth (mm), and welding time (s). The dependent variable (output) is shear load capacity (N). The data set was randomly divided into a training set (40 observations) and a test set (10 observations).

RESULTS AND DISCUSSION

SVM model quality analysis

Table 2 shows the results of training three variants of the SVM model, differing in the kernel function. It presents a comparative analysis of linear, radial basis function, and polynomial kernels, displaying the RMSE and R values for each type of kernel. Root Mean Square Error (RMSE), correlation coefficient (R), and cosine similarity (CS) index were used as measures for assessing the quality of the model [21]. The CS metric returns a value between -1 and 1, where 1 indicates the vectors are in the same direction, 0 indicates orthogonality, and -1 indicates opposite directions.

The models exhibit diverse performances, with each kernel type yielding distinct RMSE, R, and CS values. The RBF kernel and linear kernel both have a R value of 0.95, but the RBF kernel has a lower RMSE of 257.9 compared to 687.9 for the linear kernel. Although the polynomial kernel has a correlation coefficient of 0.94, it exhibits a lower RMSE of 540.8 compared to the linear kernel. All three kernel types have almost identical CS index values, and they are very high.

Choosing the superior model in this situation relies on the prioritization of performance metrics. When aiming to maximize the linear relationship between predicted and actual values by focusing on the R value, both the RBF and linear kernels perform equally well, achieving a R value of 0.95. The RMSE becomes crucial when predictive accuracy, which is the degree of similarity between predicted and actual values, is prioritized. The RBF kernel is the preferred choice because it has a much lower RMSE, suggesting greater precision in predictions.

The discrepancy between the RMSE and R values indicates that while the linear kernel effectively captures the data trend (as indicated by the high R value), its predictions, on average, deviate more from the actual values compared to the RBF kernel. The linear model may be more sensitive to outliers and have a less adaptable decision boundary compared to the RBF kernel, which is recognized for its ability to handle non-linear data patterns.

The RBF kernel model is the most balanced choice, displaying a strong correlation with the actual values and superior predictive accuracy.

Table 2. Quality assessment indicators of SVM model variants for different kernels

Kernel type	RMSE	R	Cosine Similarity (CS)
Linear	687.9	0.95	0.9953
RBF	257.9	0.95	0.9944
Polynomial	540.8	0.94	0.9963

This analysis highlights the significance of taking into account both R and RMSE when evaluating and selecting models. The RMSE demonstrates that a model with a strong correlation does not always ensure a close match between predicted and actual values. Therefore, when accurate predictions are crucial, the model with the lower Root Mean Square Error (RMSE), such as the RBF kernel in this instance, would be considered superior.

Figures 5–10 depict a graphical analysis of SVM kernel variations. This analysis combines visual and quantitative data to demonstrate the detailed effectiveness of each kernel in representing complex datasets. Figures 5 and 6 display scatter plots and regression plots using a linear kernel for 10 test cases. Figures 7 and 8 correspond to the RBF kernel, while Figures 9 and 10 refer to the polynomial kernel.

The linear kernel SVM shows a strong linear correlation between predicted and actual values, despite having a significant RMSE of 687.9, as shown in the scatter and regression plots. This error magnitude indicates significant deviations, suggesting that although the model captures the overall trend, there are still notable inaccuracies in its predictions. A correlation coefficient R of 0.95 means that the data points are close to the regression line. This means that the prediction is very accurate, and the linear connection is strong. The RMSE indicates a spread of data points significant enough to explain a considerable average error. The RBF kernel SVM shows a more intricate relationship, with a lower RMSE of 257.9 indicating a better fit to the data and therefore smaller discrepancies between the actual and predicted values. The improved performance shows that the kernel has a superior ability to capture the complexities of the dataset. The regression plot using the RBF kernel is expected to closely match the distribution of data points, with a high R value

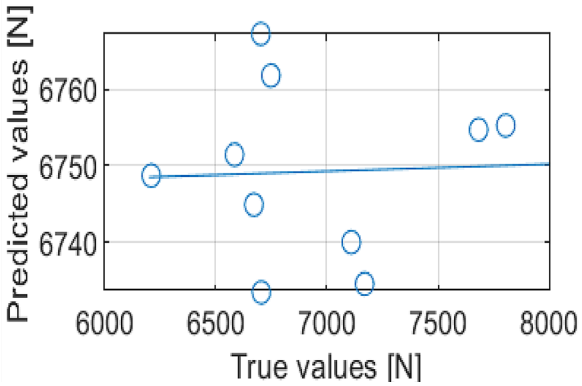

Figure 6. Regression plot of SVM with a linear kernel, RMSE = 687.9, R = 0.95

indicating a strong fit. The decreased RMSE indicates a tighter grouping of data points around the curve, demonstrating the RBF kernel's ability to adjust to the complexity of the data.

The polynomial kernel SVM strikes a balance between the simplicity of the linear model and the complexity of the RBF kernel, placing it in an intermediate position. The RMSE of 540.8 indicates moderate discrepancies between the actual and forecasted values. This moderate performance demonstrates the polynomial kernel's ability to represent relationships that are not purely linear or excessively intricate. The R value of 0.94, slightly lower than the linear and RBF kernels, along with the intermediate RMSE, indicates a dispersion pattern where data points follow the polynomial curve but have a broader distribution compared to the RBF kernel. This detailed analysis uncovers inherent compromises in choosing models for SVM applications. The linear kernel tends to have higher prediction errors even with strong linear relationships, while the RBF kernel performs better by accurately capturing complex data patterns, leading to lower deviations and tighter clustering of data points. The polynomial

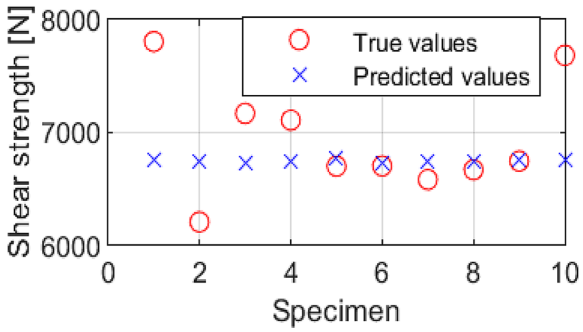

Figure 5. SVM with a linear kernel, RMSE = 687.9, R = 0.95

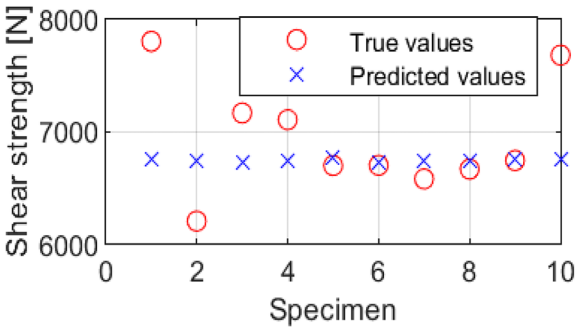

Figure 7. SVM with a RBF kernel, RMSE = 257.9, R = 0.95

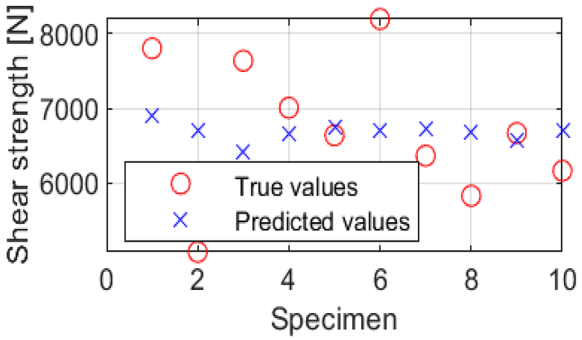

Figure 8. Regression plot of SVM with a RBF kernel, RMSE = 257.9, R = 0.95

kernel demonstrates a balanced performance in modeling various relationships, showing moderate deviations and dispersion of data points around the regression curve. The selection of kernels in SVM models is a crucial factor in optimizing model performance, underscoring the significance of kernel choice in achieving precise and dependable predictive modeling in diverse applications.

Optical investigation of the welded joint

An algorithm utilizing Otsu's thresholding method was created to enhance the inspection process of welds produced through the RFSSW technique. Nobuyuki Otsu developed the Otsu method, a global thresholding technique used to convert grayscale images into binary images [22]. The method relies on maximizing the variance between black and white pixels to minimize the variance within each class. The objective is to determine the threshold that effectively divides the pixels into two categories, foreground and background, by minimizing the variance within each category and maximizing the variance between the two categories.

Given a grayscale image, let's denote the pixels' intensities by L , where $L = 0, 1,\ldots, L\text{-}1$ (for an 8–bit image, $L = 256$). The number of pixels at each intensity level i is denoted by n_i, and the total number of pixels in the image is $N = \sum_{i=0}^{L-1} n_i$. The probability of occurrence of an intensity level in the image is given by $p(i) = \frac{n_i}{N}$

The Otsu method involves iterating through all possible thresholds and calculating the between-class variance $\sigma_B^2(t)$ for each. The optimal threshold t^* is the value of that maximizes $\sigma_B^2(t)$. The variance between classes is calculated as:

$$\sigma_B^2(t) = \omega_0(t)\omega_1(t)[\mu_0(t) - \mu_1(t)]^2 \quad (9)$$

where: $\omega_0(t)$ and $\omega_1(t)$ are the probabilities of the two classes separated by the threshold t; and $\mu_1(t)$ are the mean intensities of these two classes.

Otsu's method is highly regarded for its simplicity and efficiency in image segmentation, particularly when the image's histogram indicates a clear threshold for separating the foreground and background. This study created an algorithm utilizing Otsu thresholding. The algorithm's operation can be succinctly outlined in the following steps:

- Load the target image from a specified path.
- Convert the image to grayscale.
- Segment the grayscale image into binary using Otsu's thresholding method. Calculate and print the black-to-white pixel ratio.
- Magnify and display the grayscale image for better visualization.
- Specify the number of color levels for segmentation.
- Segment the grayscale image into the specified number of color levels.
- Convert the segmented image to a color image using a predefined color map. Optionally, swap specific colors in the segmented color image.
- Display the color-segmented image with adjustments for better visualization.
- Calculate and display the percentage of the image occupied by each color level excluding a specified background level,
- Modify the image by making the background white and recalculating color fractions excluding the background.
- Display the modified image with updated color fractions and a customized color bar.

The algorithm being discussed is designed for manipulating and analyzing images using MATLAB R2023b, a well-known environment known for its advanced image processing capabilities. The process starts with obtaining an image, which is then transformed into a grayscale version. This transformation is crucial as it simplifies the image by reducing it to a single luminance channel, making it easier to analyze and manipulate.

The script uses Otsu's method after the initial preprocessing to segment the image into a binary format by categorizing pixels as black or white based on a threshold determined automatically. The binary segmentation is important for distinguishing various features in the image. The script then quantifies this distinction by calculating the ratio of black to white pixels. This ratio provides

information about how features are spread and how common they are in the image.

The script progresses to color segmentation, starting with magnifying the grayscale image to improve visibility. The multithresh function is used to establish multiple thresholds, which results in segmenting the image into different color levels. The imquantize function applies specified thresholds to segment an image, which is then converted to a color image. This conversion simplifies distinguishing segments visually and adds complexity by assigning grayscale segments to a specific color range. The script can manipulate specific colors in the segmented image, such as swapping cyan and blue colors. This process entails detecting pixels of a specific color (cyan) and changing their color values to a designated target color (blue). The script does not include a reciprocal color swap feature, but instead concentrates on converting cyan to blue unilaterally.During later analysis stages, the script computes the proportion of the image that each color level occupies, specifically omitting a predetermined background level. This exclusion is essential to concentrate the analysis on relevant aspects of the image. The script changes the image by making the background white and adjusting the color fractions to exclude the background. This alteration highlights specific features by removing the background from the analysis. The script includes visual representations of the processed images at different stages, such as grayscale, binary, and color-segmented versions. The visual representations, along with numerical data like the proportion of each color level, offer a thorough summary of the image's characteristics and how they are spread out. The script provides a systematic method for image processing, including grayscale conversion, binary and color segmentation, color manipulation, and quantitative analysis. This complex procedure provides valuable insights into the composition and characteristics of the image, demonstrating its potential as a tool for advanced image analysis.

Assessment of weld quality based on image segmentation

Figures 11, 12, and 13 display image sets for inspecting welds. Macrostructural photos (a and d) were taken using an Opta-Tech X2000 stereoscopic microscope. Images (a–c) display the weld from a top view. Image a) displays an unedited photograph of the weld. Image b) displays the weld following binary segmentation into black and white. The absence of sufficient details hinders the practical use of this image for inspection. Image c) displays a color image of the weld divided into three color fractions. This color segmentation method enables the extraction of a greater amount of information. By analyzing the proportions of individual color fractions, we can determine the percentage share of each color in the weld image. Colors must be interpreted correctly to understand their significance. The red color marks the boundary between the metal plasticized with the welding tool and the unplasticized metal. Therefore, the minimum red color fraction can be considered an indicator of a well-executed weld. In Figure 11c, the red fraction is only 6.92%. The red color represents 10.29% in Figure 13c and 40.64% in Figure 12c, indicating a decrease in weld load capacity. Figures 11–13 (d–f) depict cross-sections of the welds displayed in images (a–c). Image d) displays a magnified unprocessed photograph of

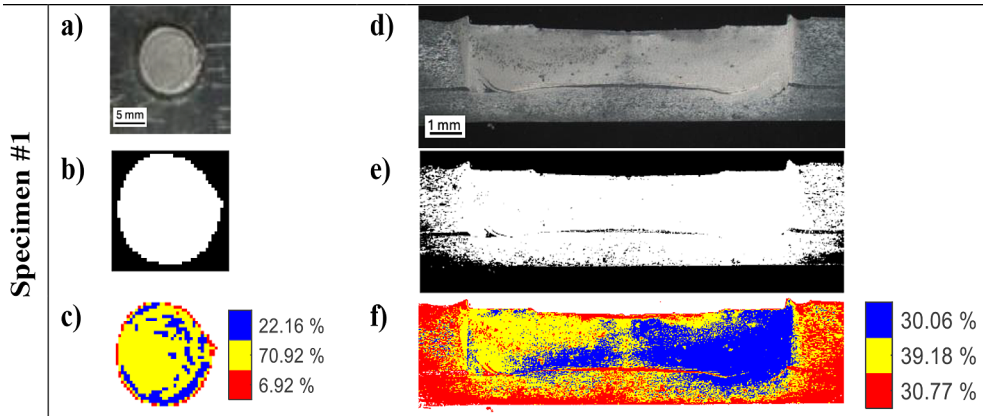

Figure 11. Inspection of the weld of specimen #1: (a) top view-photo, (b) top view-binary segmentation, (c) top view-three-color segmentation, (d) cross-section-photo, (e) cross-section-binary segmentation, (f) cross-section transverse-three-color segmentation.

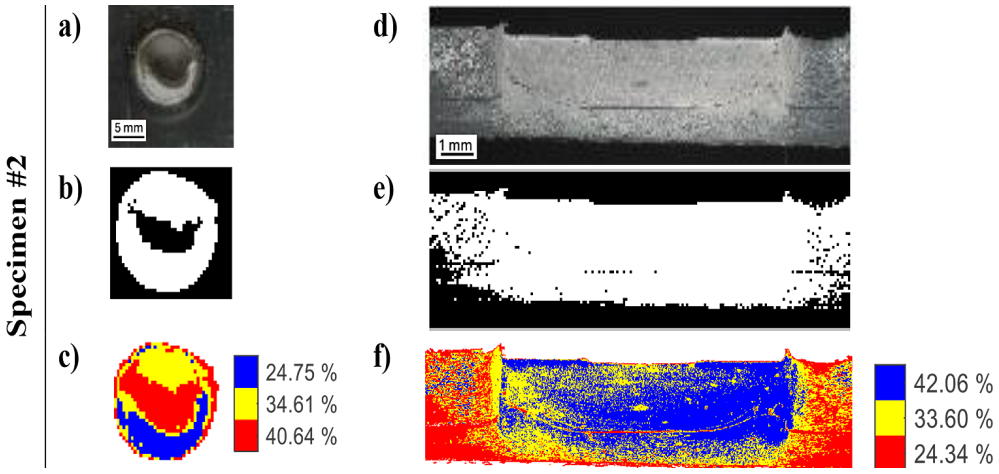

Figure 12. Inspection of the weld of specimen #2: (a) top view-photo, (b) top view-binary segmentation, (c) top view-three-color segmentation, (d) cross-section-photo, (e) cross-section-binary segmentation, f) cross-section transverse - three-color segmentation.

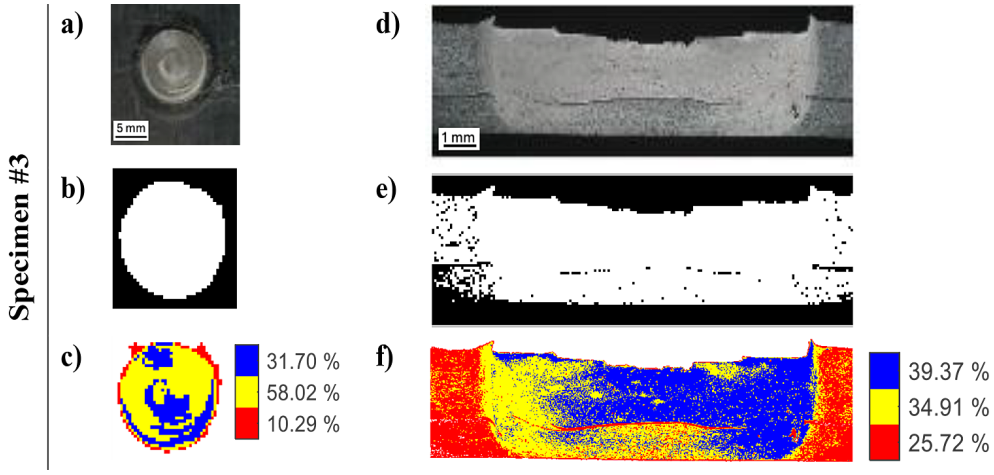

Figure 13. Inspection of the weld of specimen #3: (a) top view - photo, (b) top view-binary segmentation, (c) top view-three-color segmentation, (d) cross-section-photo, (e) cross-section-binary segmentation, (f) cross-section transverse-three-color segmentation.

the weld cross-section. Image e) is a binary graphic that contains less information than image f). The distribution of individual color fractions can only be interpreted and their percentage aspect ratios calculated in the color image f). Differences in optical equipment used to capture photos of welds from different perspectives result in variations in color interpretation between images (d–f) and images (a–c). The proposed method stands out from current quality assessment techniques primarily due to its automation and precision, facilitated by the application of machine learning and image segmentation. This automation significantly reduces the potential for human error, offering a more objective and precise assessment of weld quality. Furthermore, the SVM model's ability to predict is different from traditional methods of trial-and-error or empirical optimization. This makes it possible to choose the best welding parameters ahead of time to ensure better weld quality. The way of performing comprehensive quality assessment through detailed optical analysis goes beyond the capabilities of traditional techniques. This approach not only evaluates the physical attributes of the weld but also provides insights into quality aspects that are challenging to assess manually. The efficiency and cost-effectiveness of this automated method could lead to significant savings in time and labor for quality control processes, making it an appealing option for industries seeking to enhance their welding operations. Specifically designed to address the challenges associated with assessing the

quality of thin RFSSW joints, the proposed method meets a critical need in sectors where such joints are common. Its capacity to accurately evaluate these specialized welds underscores its potential for broad adoption in relevant industries.

CONCLUSIONS

Based on three key process parameters—tool rotational speed, tool plunge depth, and welding time—this study presents an improved method for predicting the load capacity of a weld that was made using the Refill Friction Stir Spot Welding (RFSSW) technique. The method was developed in order to improve the accuracy of the prediction. The SVM (support vector machines) machine learning method was utilized in order to train a highly effective predictive model. This model was trained on the data set that was obtained as a result of actual measurements. This is a predictive model that can be utilized as a fitness function in order to optimize the selection of welding process parameters during the RFSSW process. A visual RFSSW joint inspection technique was also developed using image segmentation based on Otsu's thresholding method. The main findings of the presented research are: Efficient optimization of welding parameters. The application of the SVM method for the optimization of RFSSW process parameters has demonstrated significant efficacy. The optimized parameters have directly contributed to enhancing the shear load capacity of the joints, a critical measure of weld quality. Predictive model performance. The SVM model, especially with the radial basis function (RBF) kernel, got an RMSE of 257.9, which shows that it was very good at figuring out how much shear load the joints could handle. Additionally, a correlation coefficient (R) of 0.95 was observed, signifying a strong linear relationship between predicted and actual values, showcasing the model's reliability. Automated quality assessment. The development of an automated quality assessment algorithm utilizing image segmentation based on Otsu's thresholding method represents a significant advancement. This technique allows for the detailed and objective analysis of weld quality, surpassing traditional manual inspection methods in both speed and precision.

Improvement over traditional techniques. The combination of the SVM predictive model and the Otsu-based image segmentation algorithm for weld inspection marks a notable improvement over existing manual and empirical methods. This advancement not only enhances the accuracy of weld quality assessment but also contributes to the efficiency of the welding process by enabling the selection of optimal parameters through automation. Potential for the Industry 4.0 revolution. The findings underscore the potential of the proposed method to revolutionize the RFSSW technique's application across various industries. By automating the optimization of process parameters and quality assessment, the presented method can significantly reduce labor intensity, costs, and duration of the welding process while simultaneously improving the quality and load capacity of the welds. RFSSW process optimization can be algorithmically automated using both the SVM predictive model and the Otsu inspection model. The RFSSW welding process typically involves the selection of optimal parameters through the use of manual labor at the present time. Automation will bring about a number of benefits, including the reduction of costs, labor intensity, and duration of the welding process, the enhancement of the quality and load capacity of the joint, and the facilitation of automation. Overall, this research presents a promising AI-based approach for welding quality assessment, offering significant improvements over existing methods in terms of automation, precision, predictive optimization, and comprehensive evaluation.

Acknowledgments

The research leading to these results has received funding from the commissioned task entitled "VIA CARPATIA Universities of Technology Network named after the President of the Republic of Poland Lech Kaczyński" contract no. MEiN/2022/DPI/2575 concluded on October 20, 2023 action entitled "In the neighborhood - inter-university research internships and study visits."

REFERENCES

1. Zhang Z, Yang X, Zhang J, Zhou G, Xu X, Zou B. Effect of welding parameters on microstructure and mechanical properties of friction stir spot welded 5052 aluminum alloy. Materials & Design 2011; 3, 2. doi:10.1016/j.matdes.2011.03.058.
2. Kubit A., Kluz R., Trzepieciński T., Wydrzyński D., Bochnowski W. Analysis of the mechanical properties and of micrographs of refill friction stir spot welded 7075-T6 aluminium sheets. Archives of Civil and Mechanical Engineering 2018; 18.

doi:10.1016/j.acme.2017.07.005.

3. Nhan PT. Effect of the welding parameters on mechanical properties of AA5083 friction stir welding. Proceedings of 5th International Conference on Green Technology and Sustainable Development, GTSD 2020. doi:10.1109/GTSD50082.2020.9303056.
4. Xiao-Jie Y., Bin W., Xiao-Yan S., Yu-Xin L. Research on adaptive control of medium frequency DC resistance spot welding. International Conference on Artificial Intelligence and Electromechanical Automation (AIEA). IEEE 2021; 30–34. doi:10.1109/AIEA53260.2021.00014.
5. Shen Z, Yang X, Zhang Z, Cui L, Li T. Microstructure and failure mechanisms of refill friction stir spot welded 7075-T6 aluminum alloy joints. Materials & Design 2013; 44: 476–486. doi:10.1016/J.MATDES.2012.08.026.
6. Kubit A., Trzepiecinski T., Bochnowski W., Drabczyk M., Faes K. Analysis of the mechanism of fatigue failure of the refill friction stir spot welded overlap joints. Archives of Civil and Mechanical Engineering 2019; 19: 1419–1430. doi:10.1016/J.ACME.2019.09.004.
7. Engineering MW-A of civil and M, undefined. Friction stir processing – state of the art. Springer MS Węglowski Archives of civil and Mechanical Engineering, 2018•Springer 2017; 18: 114–129. doi:10.1016/j.acme.2017.06.002
8. Wang X., Mu R., Wang C. numerical simulation and experimental study on self-piercing riveting of DC03/6016 dissimilar sheets. 3rd International Conference on Electron Device and Mechanical Engineering (ICEDME). IEEE 2020; 463–466. doi:10.1109/ICEDME50972.2020.00111.
9. Oh S., Kim H.K., Jeong T.E., Kam D.H., Ki H. Deep-learning-based predictive architectures for self-piercing riveting process. IEEE Access 2020; 8: 116254–116267. doi:10.1109/ACCESS.2020.3004337.
10. Mubiayi M.P., Akinlabi E. Titilayo, Makhatha M.E. Effect of process parameters on tensile strength and morphology of friction stir spot welds of aluminium and copper. 8th International Conference on Mechanical and Intelligent Manufacturing Technologies (ICMIMT). IEEE 2017; 48–53. doi:10.1109/ICMIMT.2017.7917433.
11. Mahgoub A., Merah N., Bazoune A., Al-Badour F. Effect of pin tool profile on mechanical and metallurgical properties in friction stir spot welding of pure copper. 8th International Conference on Mechanical and Aerospace Engineering (ICMAE). IEEE 2017; 381–384. doi:10.1109/ICMAE.2017.8038676.
12. Pizoń J., Gola A. The meaning and directions of development of personalized production in the era of industry 4.0 and Industry 5.0. Lecture Notes in Mechanical Engineering 2023; 1–13. doi:10.1007/978-3-031-09360-9_1/COVER.
13. Kozłowski E., Antosz K., Sęp J., Prucnal S. Integrating sensor systems and signal processing for sustainable production: analysis of cutting tool condition. Electronics 2024; 13, 185. 2023; 13: 185. doi:10.3390/ELECTRONICS13010185.
14. Lonkwic P., Tofil A. Supporting welding work in the aspect of increasing production process efficiency. Advances in Science and Technology Research Journal 2023; 17: 8–14. doi:10.12913/22998624/157418.
15. Kulisz M., Kłosowski G., Rymarczyk T., Słoniec J., Gauda K., Cwynar W. Optimizing the neural network loss function in electrical tomography to increase energy efficiency in industrial reactors. Energies (Basel) 2024; 17: 681. doi:10.3390/EN17030681.
16. Kulisz M., Kujawska J., Aubakirova Z., Zhairbaeva G., Warowny T. Prediction of the compressive strength of environmentally friendly concrete using artificial neural network. Applied Computer Science 2022; 18. doi:10.35784/acs-2022-29.
17. Kłosowski G., Rymarczyk T., Niderla K., Rzemieniak M., Dmowski A., Maj M. Comparison of machine learning methods for image reconstruction using the LSTM classifier in industrial electrical tomography. Energies 2021; 14, 7269. doi:10.3390/EN14217269.
18. Rymarczyk T., Kłosowski G., Cieplak T., Niderla K. The use of dual machine learning in industrial electrical tomography. Journal of Physics: Conference Series 2022; 2408: 012023. doi:10.1088/1742-6596/2408/1/012023.
19. Chen K., Yao H., Han Z. Arithmetic optimization algorithm to optimize support vector machine for chip defect Identification. 28th International Conference on Mechatronics and Machine Vision in Practice (M2VIP). IEEE 2022; 1–5. doi:10.1109/M2VIP55626.2022.10041106.
20. Sánchez VDA. Advanced support vector machines and kernel methods. Neurocomputing 2003; 55. doi:10.1016/S0925-2312(03)00373-4
21. Olaseni K, Aliyu S, Bakare K. A fuzzy c-means news article clustering based on an improved sqrt-cosine similarity measurement. Science Forum (Journal of Pure and Applied Sciences) 2022; 22. doi:10.5455/sf.olasamkay.
22. Ghanbari T., Mehraban A. Data threshold setting using a new approach based on otsu's image thresholding. International Conference on Protection and Automation of Power Systems (IPAPS). IEEE 2022; 1–5. doi:10.1109/IPAPS55380.2022.9763224.